JOURNAL OF MATERIALS SCIENCE 28 (1993) 6167–6177

Fracture toughness and fracture mechanisms of PBT/PC/IM blend

Part II *Toughening mechanisms*

JINGSHEN WU, YIU-WING MAI
Centre for Advanced Materials Technology, Department of Mechanical Engineering, University of Sydney, New South Wales, 2006, Australia

Scanning electron microscopy (SEM) and transmission electron microscopy (TEM) techniques were employed in the morphology and fracture mechanisms studies on a commercial polybutylene terephthalate/polycarbonate/impact modifier (PBT/PC/IM) blend. The fracture mechanisms involved at different temperatures under both impact and static loading were revealed. It was found that massive plastic deformation of the matrix material occurred *after* rubber particle cavitation; and it was this plastic deformation that was responsible for the drastic enhancement in fracture toughness although the widespread cavitation did absorb a considerable amount of energy as well. The major source of toughness was the same for both impact and static fracture tests, but the toughening processes became effective at a much lower temperature under static than impact conditions. The sequence of toughening events was also observed using TEM.

1. Introduction

It is well known that substantial enhancement in toughness of a brittle polymer can be achieved by blending it with rubber particles [1]. Conventional polymer blends, such as High Impact Polystyrene (HIPS), Polyamide (PA)/rubber and epoxy/rubber, normally include two phases, e.g. a brittle polymer matrix with elastomer inclusions. Tremendous efforts on revealing the mechanisms responsible for the dramatic toughness increment have been made in the past [1–27]. The mechanisms suggested are multiple crazing [2], shear yielding [3, 4], crazing with shear yielding [5] and rubbery particle stretching and tearing [6, 7]. A large amount of experimental evidence exists to prove that the mechanisms listed above act during the fracture process of toughened polymers either individually or cooperatively. A commonly accepted view on the role of rubbery particles is that the rubber inclusions alter the stress state in the material around the particles and induce extensive plastic deformation in the matrix, such as multiple crazing and shear bands or both. In general, the massive plastic deformation in the matrix is believed to absorb a major part of the total fracture energy though the rubber particle deformation itself does make a small contribution to the toughness. Because the stress condition around the particles is particularly important in respect of activating matrix plastic deformation, the effects of rubber particle size [8–10], inter-particle distance [9, 11] and particle cavitation behaviour [12–14] have received considerable attention. The effect of particle size on the fracture toughness depends on the nature of the matrix. It is proposed that materials with a propensity to crazing prefer particles larger than 1 μm, whereas shear deformation in a ductile polymer matrix is favoured by particles smaller than 1 μm. The inter-particle distance criterion is proposed by Wu based on his work with rubber toughened nylon [9, 11]. He suggests that rubber particles change the stress field in the matrix around the particles and when the inter-particle distance is smaller than a critical value, which is a constant for a given matrix, the overlapping stress fields between the neighbourhood particles result in extensive shear deformation. The rubber particles in this model only act as stress concentration points. The model is supported by some experimental work and finite element method (FEM) analysis [15]. The importance of rubber particle cavitation was first noticed by Yee and co-workers [16–18]. Although the massive plastic deformation in the matrix is admitted as the major energy absorption mechanism, however, rubber cavitation and especially the sequence of cavitation and shear deformation is emphasized [12–14]. It is shown that cavitation of the rubbery particles is the first step of the fracture processes. It relieves the plane strain constraint to allow the matrix between the particles to undergo shear yielding because the matrix material between the cavities is in a plane stress condition. It is believed that without rubber cavitation only very limited shear deformation can occur. Although a considerable amount of experimental work has confirmed the presence of rubber cavitation [19–21] and the sequence of cavitation/shear yielding [12–14, 22], the necessary condition of cavitation prior to shear yielding for toughening is still in debate [23–27].

The toughness enhancement of traditional polymer blends is often achieved at the expense of some other

important mechanical properties, such as stiffness, modulus and heat resistance. A solution to this problem is partly reached by blending more than two types of polymer together, and in many cases the newly developed blends generally include two rigid polymers and one elastomer, among them are PA/PPO (Polyphenylene Oxide)/elastomer, PBT (Polybutylene Terephthalate)/PC (Polycarbonate)/elastomer, PC/ABS (Acrylonitrile-butadiene-styrene) and PS (Polystyrene)/PPO [28–32]. Most of the new blends are featured not only by high toughness but also by, for instance, high chemical resistance, high heat-distortion temperature, low moisture absorption and excellent electrical properties. Strength and modulus reduction is minimized and processing becomes easier. In spite of their important engineering applications, only very limited work has been done on their mechanical properties and toughening mechanisms involved in fracture processes. Apparently, a systematic study on the blends is needed to reveal the secret of the toughening processes and set up a clear criterion for the development of new polymer blends.

In Part I of this paper [33] the fracture toughness behaviour of a commercial polymer blend, polybutylene terephthalate (PBT) polycarbonate (PC)/impact modifier (IM) were reported. The toughness of the blend was measured under different temperatures and strain rates and their effects were discussed. In this part of the paper the major interest is to explore the toughening mechanisms beneficial to the enhancement of toughness. The study was carried out by optical microscopy (OM), scanning electron microscopy (SEM) and transmission electron microscopy (TEM) with OsO_4 stained samples. Single-edge notched bend (SENB) specimens were employed to create the required deformation zone in front of a crack tip under both static and impact loading at different temperatures. The cold-section technique was used to reveal the sub-surface deformation inside the fractured samples.

2. Experimental procedure

2.1. Material and specimen preparation

The blend used in this study was the same commercial blend employed in Part I of the paper for the fracture toughness tests [33].

Both sub-fracture surface and original fracture surface from the mechanical tests were prepared for fracture mechanisms study. The sub-fracture surface was created by the cold-section technique [20]. As illustrated in Fig. 1, prior to cold-section, specimens with notches on one side were subjected to low-energy impact or statically bent until crack initiation occurred which usually coincided with the point of non-linearity in the load–displacement curve. At low temperatures this technique did not work. One crack would run unstably but the other crack would be arrested with very little crack growth [22]. The part of the sample with arrested crack was renotched in the mid-thickness direction perpendicular to the crack plane and then immersed in liquid nitrogen for 20 min followed by a fast wedge-in fracture. The sequence of preparation is detailed in Fig. 1.

The sub-fracture surface as well as fracture surface were plated with gold before being studied in a JOE 35C SEM. The specimens specified for the study of morphology under SEM were also plasma etched for a few minutes before being coated with gold. Samples for optical microscopic examinations were cut to 2–5 μm thickness with a Reichart Ultracut E ultramicrotome.

The ultra-thin sections for TEM analysis were sliced from the top of a block trimmed from a cold-sectioned

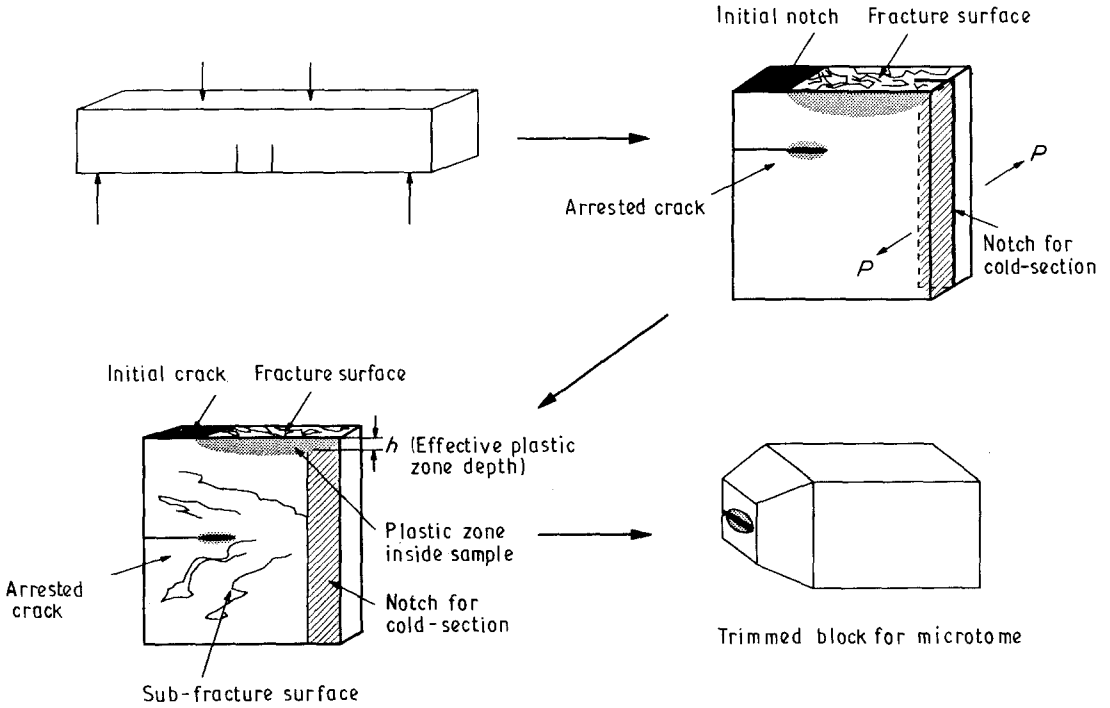

Figure 1 Schematic drawing of the cold-section process and preparation of samples for TEM study.

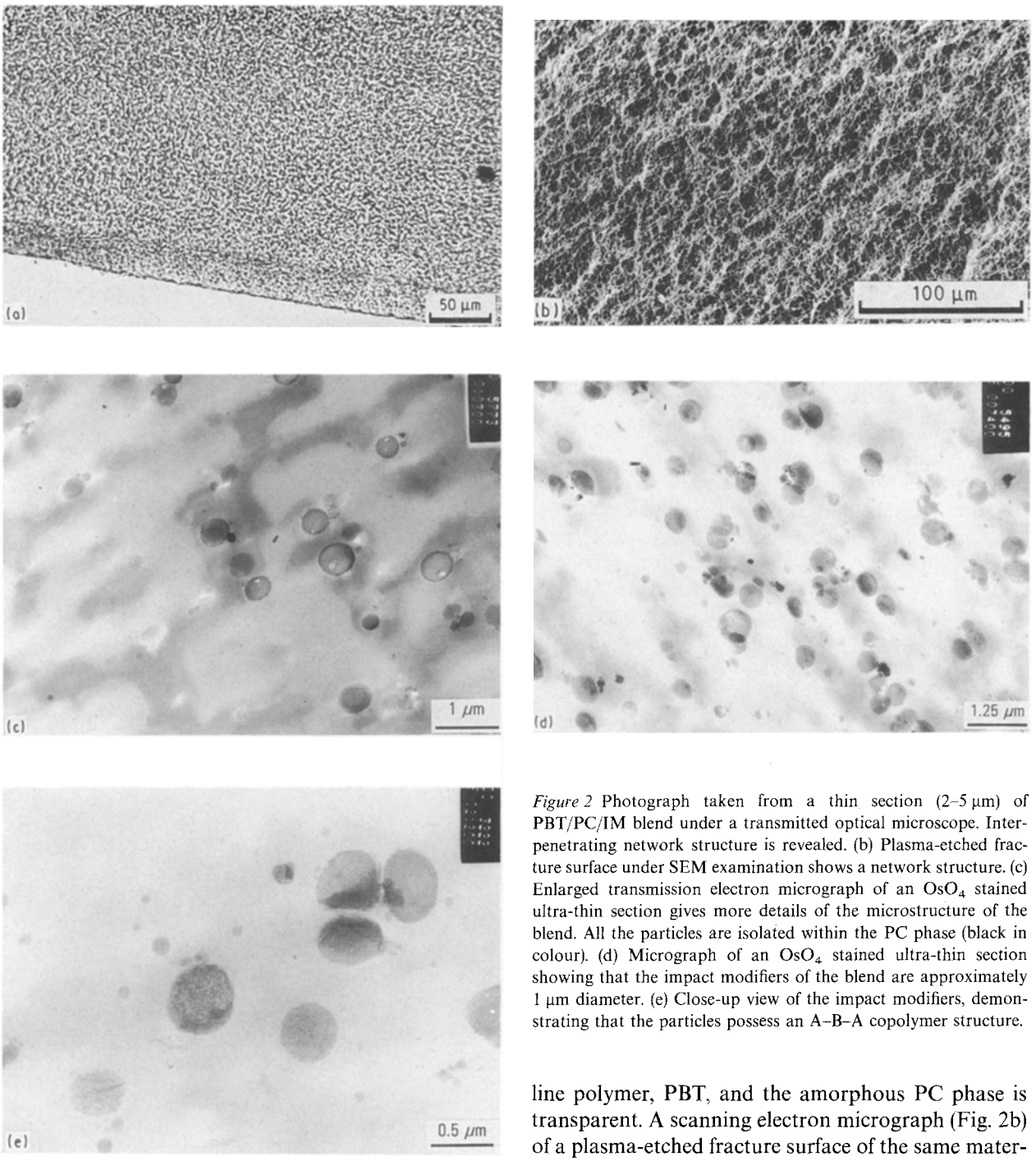

Figure 2 Photograph taken from a thin section (2–5 μm) of PBT/PC/IM blend under a transmitted optical microscope. Interpenetrating network structure is revealed. (b) Plasma-etched fracture surface under SEM examination shows a network structure. (c) Enlarged transmission electron micrograph of an OsO_4 stained ultra-thin section gives more details of the microstructure of the blend. All the particles are isolated within the PC phase (black in colour). (d) Micrograph of an OsO_4 stained ultra-thin section showing that the impact modifiers of the blend are approximately 1 μm diameter. (e) Close-up view of the impact modifiers, demonstrating that the particles possess an A–B–A copolymer structure.

specimen, Fig. 1. Each block contained an intact sub-fracture surface with a complete arrested crack tip surrounded by a stress-whitening zone. The blocks were stained in a 2% OsO_4 water solution with the sub-fracture surface down for a few days. Again, a Reichart Ultracut E ultra-microtome was used to section TEM specimens with thicknesses from 80–100 nm. The thin sections were then mounted on copper grids for subsequent examination in a Phillips E430.

3. Results and discussion

3.1. Morphology study

A photograph of the PBT/PC/IM blend taken by an optical microscope is shown in Fig. 2a. It suggests that this unique material possesses a bicontinuous microstructure. The black phase represents the semi-crystalline polymer, PBT, and the amorphous PC phase is transparent. A scanning electron micrograph (Fig. 2b) of a plasma-etched fracture surface of the same material supports this conclusion. An enlarged transmission electron micrograph of an OsO_4 stained specimen, Fig. 2c, reveals the same microstructure and furthermore, it indicates that the elastomer particles are mostly isolated in the PC phase which is black in the picture because PC is easier to stain than PBT [34, 35]. These observations are in agreement with Hobbs *et al.* [31] and Delimoy *et al.* [36]. The impact modifier used is approximately 0.5 μm diameter (Fig. 2d). An enlarged view of the IM particles in Fig. 2e shows that the particle has a core-shell structure. The core of the particle is rubbery in nature, which appears to be darker because its unsaturated chemical bonds are easier to be oxidized by OsO_4.

3.2. Fracture mechanisms

3.2.1. SEM analysis of fracture processes in impact tests

Direct observations on the fracture surfaces obtained

in impact tests at different temperatures shows the presence of three types of surface, namely brittle, semi-brittle and ductile fracture surfaces.

The brittle fracture surfaces are observed at − 196 and − 100 °C. As shown in Fig. 3a, the surface of this type possesses distinctive fast-fracture features, e.g. smooth crack-initiation point at the razor notch root followed by a hackled fast surface [37]. Very limited stress whitening can be seen on the crack initiation point in enlarged scanning electron micrographs in Fig. 3b and c, which is caused by the small voids formed by rubber-particle debonding and stripping off. No significant plastic deformation is sighted over the entire surface. This might be the reason for low toughness of the blend when it is tested in this temperature range.

The semi-brittle fracture surfaces observed at − 60, − 30 and 0 °C are essentially the same. The surface consists of a whitened zone followed by an area of fast fracture. The difference between the surfaces at different temperatures is that the low temperature has a smaller whitened zone. Thus the fracture surface of − 60 °C contains a very narrow whitened strip near the notch root whereas that of 0 °C has a relatively large whitened zone of approximately one-third of the entire fracture surface. A photograph of the fracture surface at − 30 °C is shown in Fig. 4a which is relatively smooth compared to Fig. 3a. A narrow stress-whitened strip is clearly seen in Fig. 4b. The microstructure of this zone given in Fig. 4c shows that the stress whitening in this area is a result of cavitation and matrix tearing. Hence, crack propagation at these temperatures can be divided into two steps, i.e. slow crack growth in the whitening zone followed by an unstable fast crack propagation which generates a fracture surface as shown in Fig. 4d. During slow crack growth the crack tip is blunted by the plasticaliy deformed material giving a higher crack-initiation resistance [33].

When the test temperature reaches room temperature, ductile fracture occurs. The fracture surface generated in this situation is unique and useful for understanding the toughening mechanisms. As can be seen in Fig. 5a and b, the extensive stress whitening can be observed not only on the fracture surface but also on the side of the sample beneath the crack plane. The fracture surface now has two areas with different appearance. The inner one, zone I in Fig. 5a, is further discovered by SEM to have a highly cavitated structure. The pictures taken from the crack-initiation point and the centre of the zone are shown in Fig. 5c and d. A large amount of voids with 3–10 μm diameter spreads all over the area and some spherical particles can be found occasionally. The information derived from these pictures suggests that massive cavitation happened inside the rubbery particles as well as at the boundary between matrix and inclusions. Recall that the rubbery particles have a size of approximately 1 μm diameter, whereas most of voids in this area are 5–10 times larger than the original particles. It is, therefore, a reasonable assumption that the coalescence of neighbouring voids initiated by individual particles must have occurred. Apparently, the material

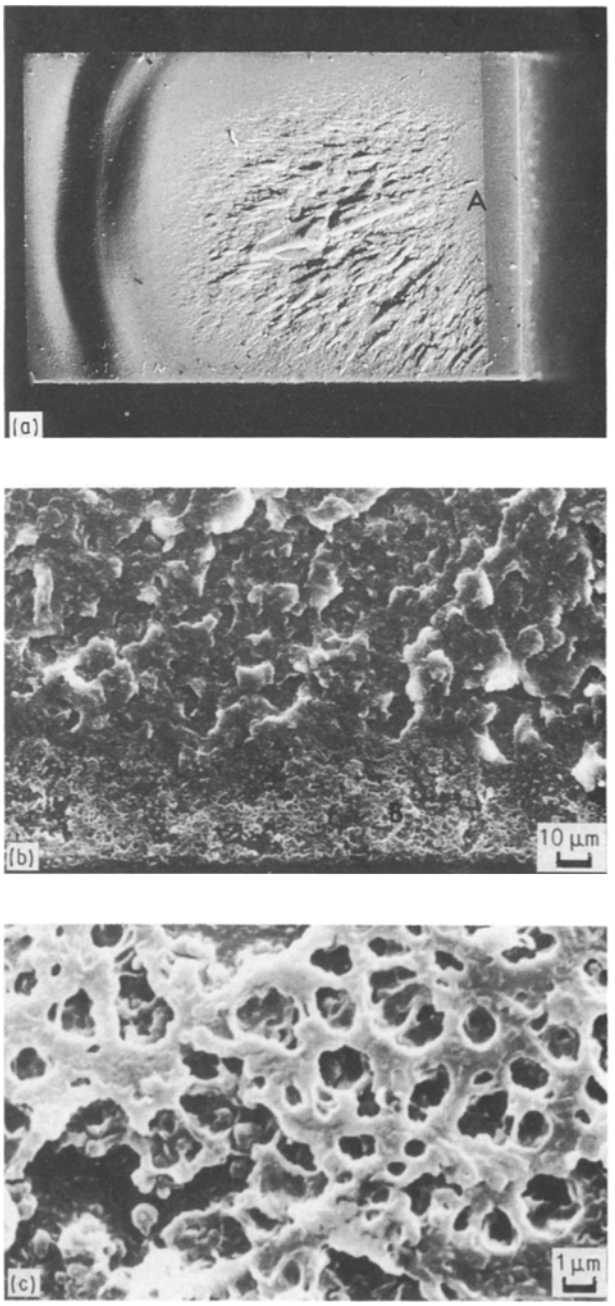

Figure 3 The entire fracture surface obtained in an impact test test carried out at − 196 °C, × 10. (a) Enlarged scanning electron micrograph of zone A in (a). (b) Enlargement of zone B in (b).

in zone I is subjected to plane strain as the specimen is bent and hence the particles in the area are triaxially stretched during loading. As soon as the rubber tearing strength or matrix–particle debonding strength is reached, cavitation occurs, and subsequently, the thickness of the polymer material between the neighbouring voids is reduced gradually until the thinnest part is totally broken so that the neighbouring voids form one big void. Fig. 5e and f show a very large void formed by several small voids and the fibrils of the polymer walls are still visible. The outer area of the fracture surface, zone II in Fig. 5a, is featured by a set of parabolic markings starting at the boundary of zones I and II. The parabolic markings are known to result from the disturbances of secondary crack initiations [38]. A scanning electron micrograph taken from this zone, Fig. 5g, reveals a typical

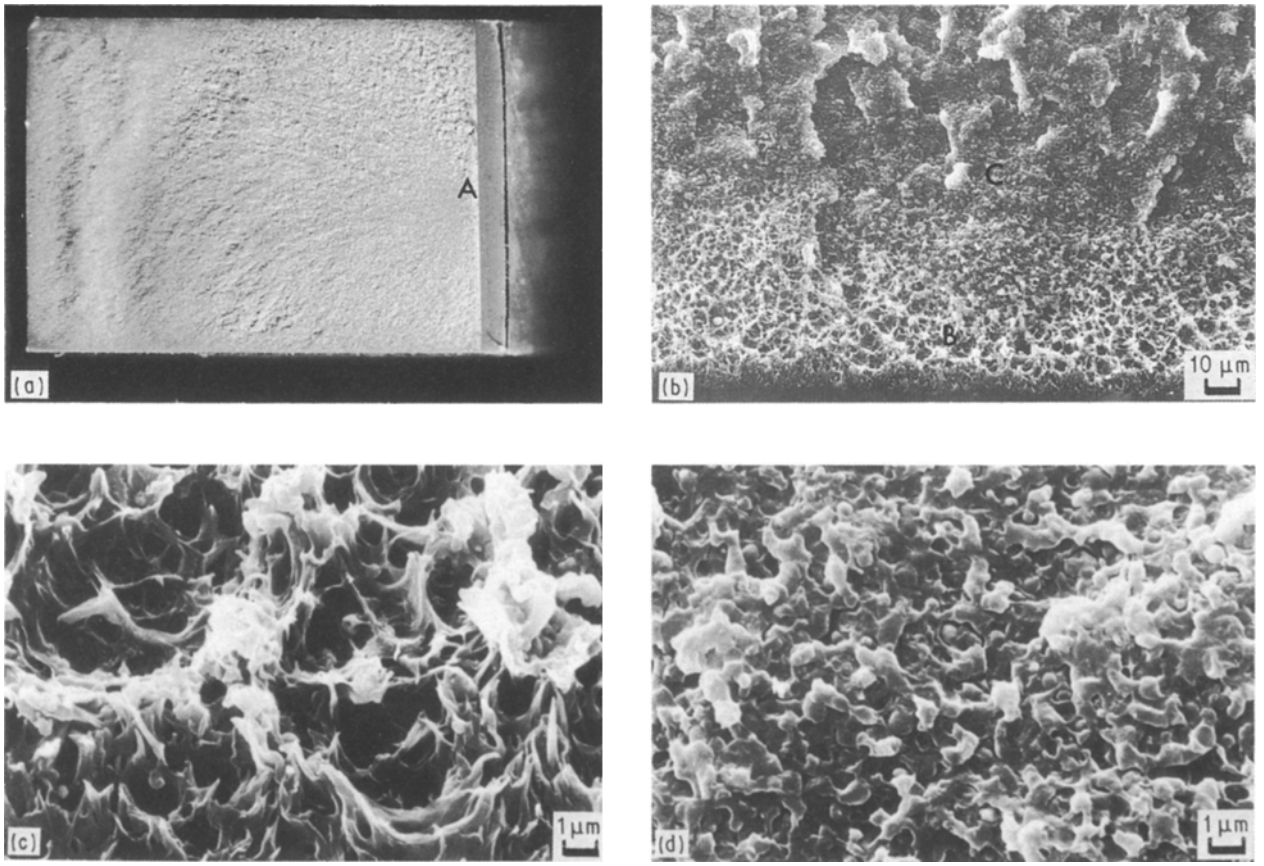

Figure 4 (a) The entire fracture surface obtained in an impact test carried out at − 30 °C, × 10. (b) Enlarged scanning electron micrograph of zone A in (a). (c) Enlargement of zone B in (b). (d) Enlargement of zone C in (b).

fibrillated structure originated from the ductile tearing of the ligament of voids. It is not surprising that no evidence of coalescence of voids can be seen because zone II is mainly subjected to plane stress during loading. The initiated voids in this stress state cannot dilate triaxially but are non-uniformly stretched in the principal stress direction instead. The ductile tearing of the ligament between particles forms the fibrils observed in Fig. 5g. In conclusion, the deformation events discerned in the fracture process are cavitation, void coalescence and ductile tearing of ligaments between voids. These events do not only occur on the fracture surface but are also spread out in areas remote from the crack plane. A tremendous energy is absorbed during these deformation processes, especially during the matrix ductile tearing, and as a result, the toughness of the blend is drastically enhanced.

At even higher temperatures, the fracture surface has only one structure (Fig. 6a and b) which is similar to the micro-structure of zone II in Fig. 5a, indicating that once the voids are initiated, ductile tearing of the matrix in the main stress direction occurs immediately because the yield stress of the blend is reduced at high temperatures and shear yielding of the ligament between the voids become easier.

These three types of fracture surfaces obtained at different temperatures coincide with the variation of impact toughness with temperature reported in Part I [33]. The lowest toughness was found at − 196 and − 100 °C and the fracture surfaces in this circumstance were typical fast-fracture surfaces without detectable plastic deformation. The slight fracture toughness increase in the temperature range − 60 to − 30 °C could now be related to the stress-whitened strip found in the micrographs. Possibly, the limited plastic deformation at the notch root was caused by the movement of polymer long-chain segments because the test temperature is about the same as the polymer relaxation peak and the T_g of the rubbery particles. The triaxial stress is high at the notch root, which promotes localized cavitation and ductile tearing of the ligament between the voids. The large toughness obtained at room temperature or higher is clearly a result of massive cavitation and extensive shear yielding discussed in the foregoing. The crack tip is severely blunted, as shown in Fig. 7, due to the plastic flow in its vicinity.

3.2.2 SEM analysis of static SENB tests

In general, the fracture surfaces obtained in the static SENB tests can be classified into two kinds. A partially stress-whitened fracture surface was found at − 196 and − 100 °C and overall stress whitening was observed at − 60 °C and higher. Note that in the impact tests, gross stress whitening did not occur until room temperature.

A set of micrographs taken from the fracture surface at − 196 °C in the SENB tests demonstrates that the

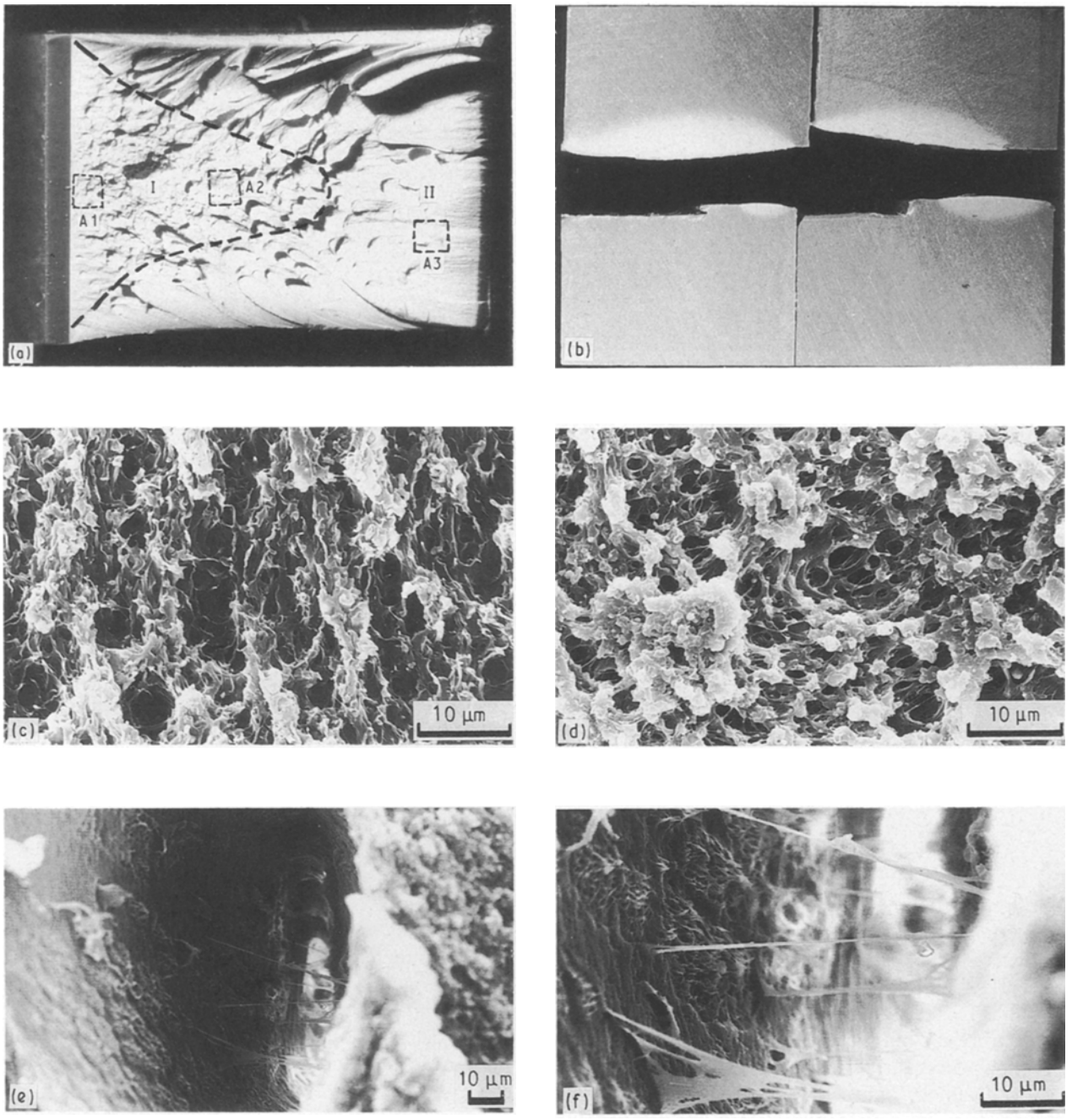

Figure 5 (a) Complete fracture surface obtained in an impact test carried out at room temperature. Two different fracture appearances are clearly seen in zones I and II, × 16. (b) Side view of broken samples from impact tests at room temperature. Stress whitening extended to the material beneath the crack surfaces, × 9. (c) Scanning electron micrograph of area A1 in (a). Large voids are formed from coalescence of smaller voids. (d) Scanning electron micrograph of area A2 in (a). (e) Enlargement of a large void in zone I of (a). (f) Fibrils of polymer material between neighbouring small voids. (g) Enlargement of area A3 in zone II of (a).

deformation behaviour of the material in the stress-whitened strip (Fig. 8a) near the notch root is very similar to that found in Fig. 4c showing cavitation and tearing. Therefore, when this blend is tested under static loading, slow crack growth can occur even at – 196 °C. The pictures taken from outside this whitened zone, Fig. 8b and c, are similar to Fig. 4d, showing fast unstable crack propagation.

Overall stress whitening of the fracture surface obtained at – 60 °C and higher temperatures is due to the widespread cavitation and ductile tearing. The photographs taken from a fracture surface at – 30 °C, Fig. 9a–c, substantiate this conclusion and they are similar to Fig. 5g. Evidently, the source of toughness is

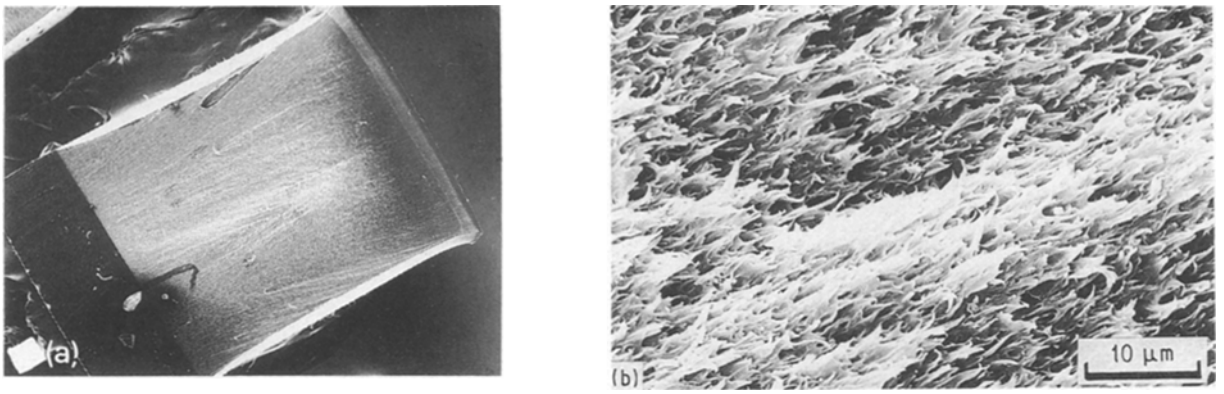

Figure 6 (a) The complete fracture surface of a sample broken in an impact test at 70 °C × 10. (b) Fibrillated structure found in the crack initiation region in (a).

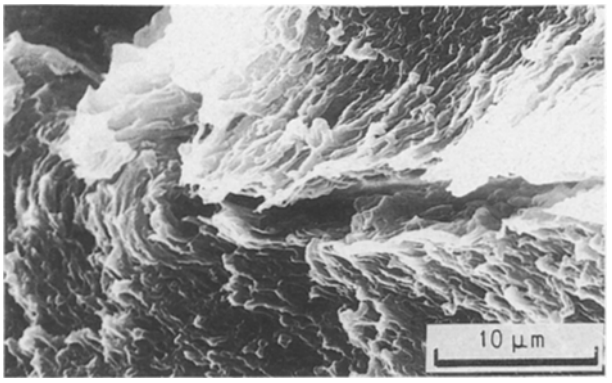

Figure 7 Scanning electron micrograph of a sub-fracture surface of an impact loaded specimen at 70 °C and an arrested crack tip. Crack-tip blunting is severe and clearly shown.

the same for both impact and static fracture toughness. However, the same toughening process becomes effective at a very much lower temperature in the static test condition than in the impact situation. This again confirms the time–temperature equivalence relationship for the fracture toughness discussed in Part I [33].

3.2.3. TEM study on fracture mechanisms

Although the SEM studies of the fracture surfaces have given a clear picture of the energy-dissipation processes responsible for the enhancement in toughness, the sequence of events cannot be ascertained from scanning electron micrographs. In addition, the deformation behaviour of the material underneath the fracture surfaces, for both brittle and ductile fractures, still remains unclear. In order to solve this problem, a set of TEM specimens was prepared to examine the relationship between the toughness and material deformation behaviour beneath the fracture surfaces.

The photographs shown in Fig. 10a–d were taken from the different locations on an ultra-thin section cut from a SENB specimen that was only partially cracked at room temperature. The sequence of deformation events can be studied here. The first step of the sequence is particle cavitation and matrix crazing, as shown in Fig. 10a. There is no shear yielding in the matrix around the cavitated particles and hence the particles are spherical. Some crazes are visible. Both particles and crazes are shown in black because of OsO_4 staining. Fig. 10b, taken from an area close to the crack tip, gives the second step in the sequence, which consists of cavitated particles distorted in the loading direction, implying that the polymer material between the voids has undergone shear yielding to some extent and the plane strain condition is partially relieved. The proof of extensive shear deformation of the matrix material between voids is demonstrated in Fig. 10c. In this transmission electron micrograph the black rubbery inclusions are elongated in the principal stress direction for several hundred per cent and the fracture surfaces are laterally pressed together forming the black rubbery strips. Even more severe deformation of the rubbery inclusions is observed around the blunted crack tip, Fig. 10d, indicating the occurrence of heavy plastic flow of matrix in this step of the deformation process.

TEM was also used to study the fracture process in an impact-loaded sample at room temperature. The transmission electron micrographs of the region near the arrested crack tip are given in Fig. 11a–c. Here, only rubber cavitation and matrix crazing can be seen, Fig. 11a. The cavitated particles remain essentially spherical even though the volume dilation of the particles is obvious. There is no sign of any shear deformation to be seen even in the vicinity of the crack tip (Fig. 11b and c). The crack tip is sharp and there are a few fibrils due to the collapse of voids detected on the fracture surface.

As has been indicated in Section 3.2.1, there are two zones in the room-temperature impact fracture surface (see Fig. 5a). The inner zone is formed under plane strain condition and the particles in this region are subjected to high triaxial stresses which promote volume-increasing processes such as cavitation and crazing. When preparing the TEM sample, crack propagation is always stopped after very small crack growth. Thus, the details seen in Fig. 11 are similar to zone I of Fig. 5a.

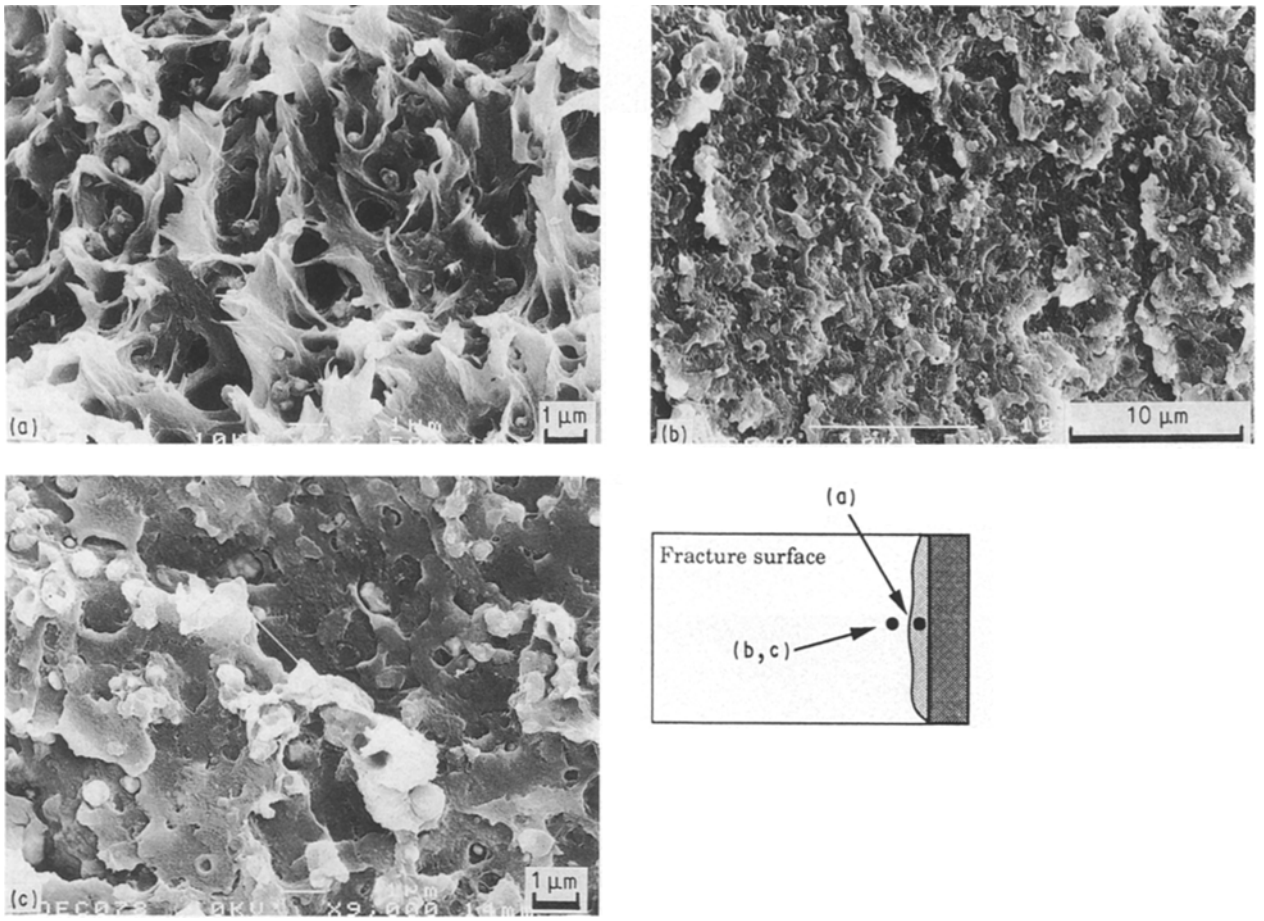

Figure 8 (a–c) Scanning electron micrographs taken from various locations of the fracture surface obtained in a statically loaded specimen carried out at − 196 °C.

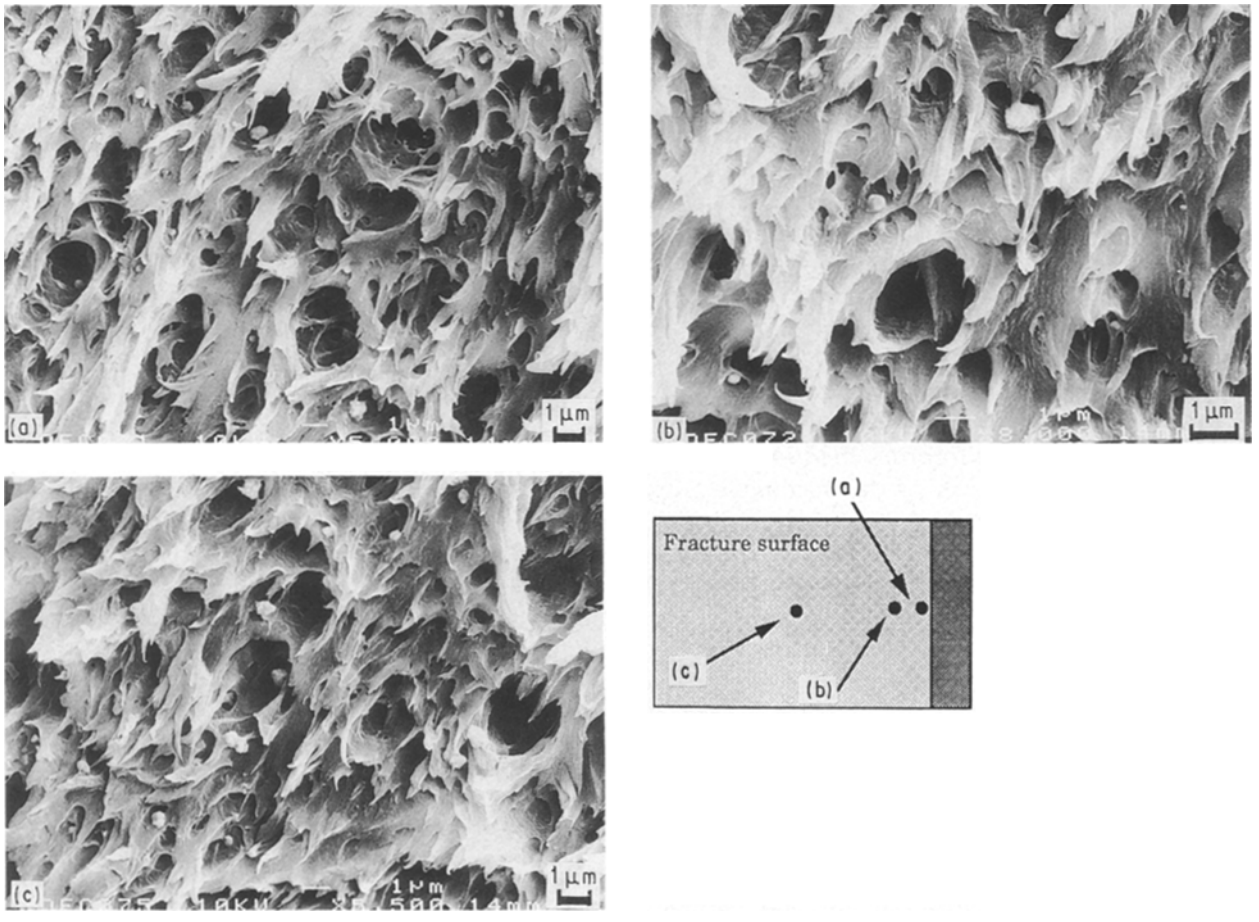

Figure 9 (a–c) Scanning electron micrographs taken from various locations of the fracture surface obtained in a statically loaded SENB specimen carried out at − 30 °C.

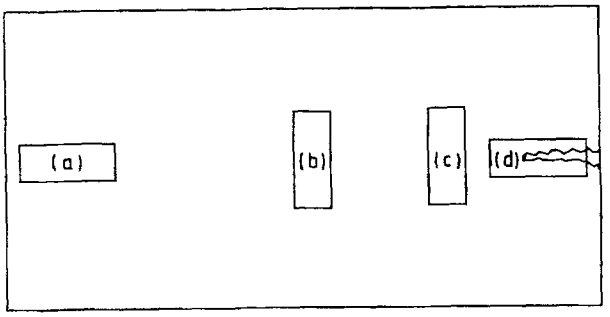

Locations of photos from crack tip

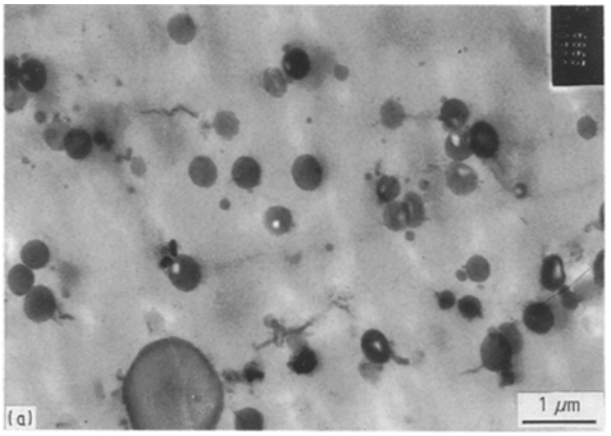

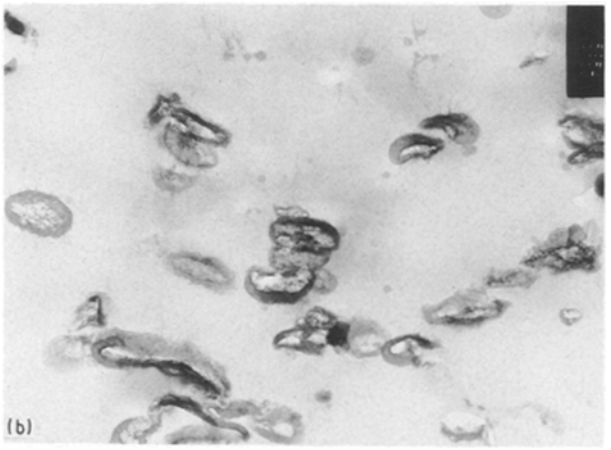

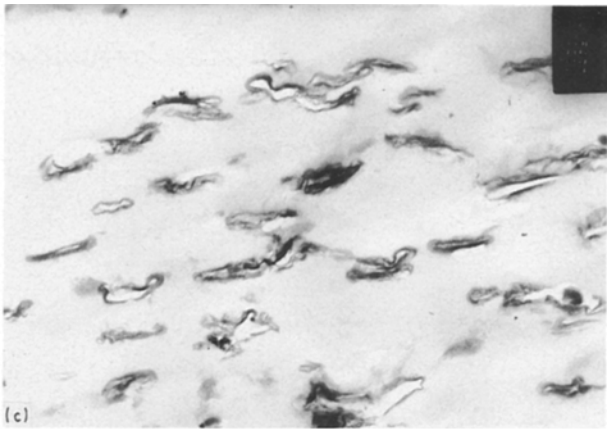

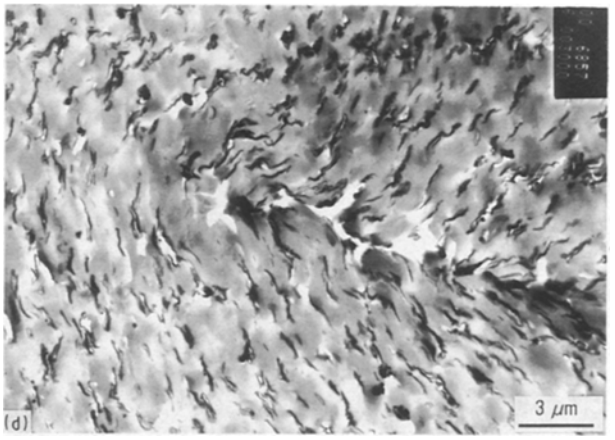

Figure 10 (a–d) Transmission electron micrographs taken from an ultra-thin section of a statically loaded sample at room temperature. The sequence of fracture mechanisms can be seen from the set of photographs shown (a)–(d) corresponding to the locations (a–d) indicated near the crack tip. Details are given in the text. (b) × 17 100, (c) × 10 300.

At an elevated temperature (70 °C) under impact loading, the same sequence of fracture events can be obtained as that for a SENB specimen subjected to static loading (see Fig. 12a–c). Crazing however, is not found at this temperature, which suggests that the shear yielding stress is lower than the crazing stress; but it is still higher than the rubber tearing stress so that cavitation remains.

4. Conclusions

To sum up the observations obtained from OM, TEM and SEM studies, we may conclude as follows.

1. The PBT/PC/IM blend has an inter-penetrating network structure with the impact modifiers isolated within the PC phase and the particles have an A–B–A copolymer micro-structure.

2. The stress whitening observed on the fracture surface is a result of massive cavitation and extensive ductile tearing of the matrix. The cavitation occurs inside the IM particles as well as at the boundary of particle and matrix.

3. Matrix shear yielding is the major energy dissipation process, although cavitation also absorbs considerable energy.

4. The variation of fracture toughness with temperature is directly related to the variation of stress-whitening zone size with temperature. The larger the stress whitened zone, the higher is the fracture toughness.

5. The same source of fracture toughness is found in both impact and static tests, but the toughening processes become effective at a much lower temperature in the static test condition than in impact. Time–temperature superposition holds for the fracture toughness–temperature relationship.

6. The sequence of toughening events is found via TEM study. In ductile fracture the sequence is first cavitation and crazing without shear yielding, then dilation of the cavitated particles together with some extensive shear in the matrix, then massive shear flow in the matrix, and finally very large elongation of the

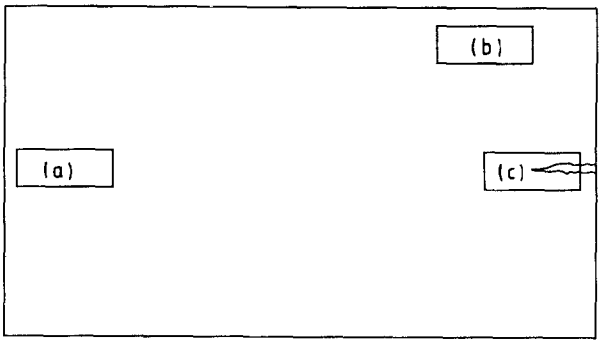

Locations of photos from crack tip

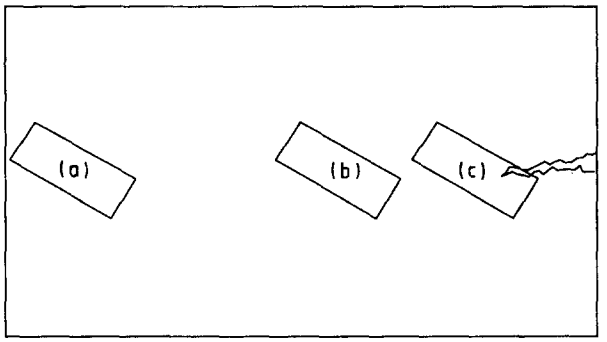

Locations of photos from crack tip

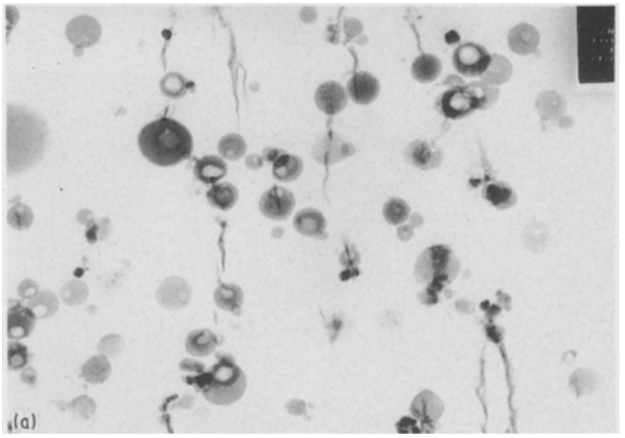

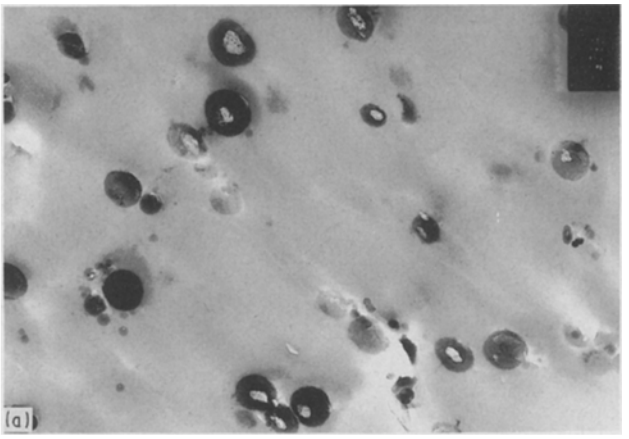

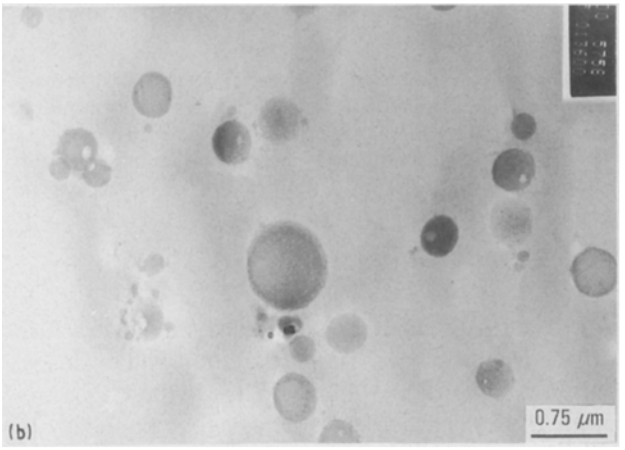

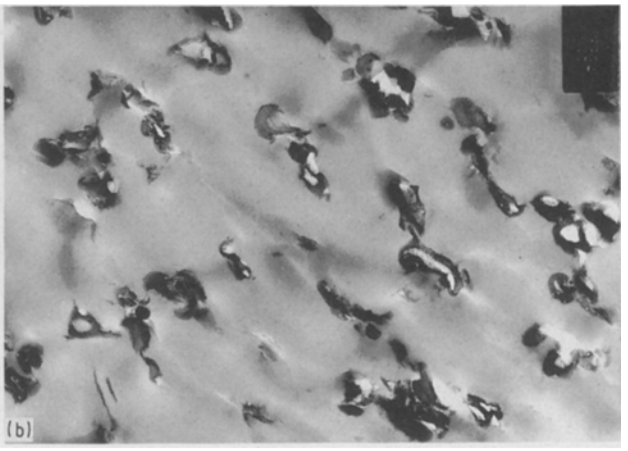

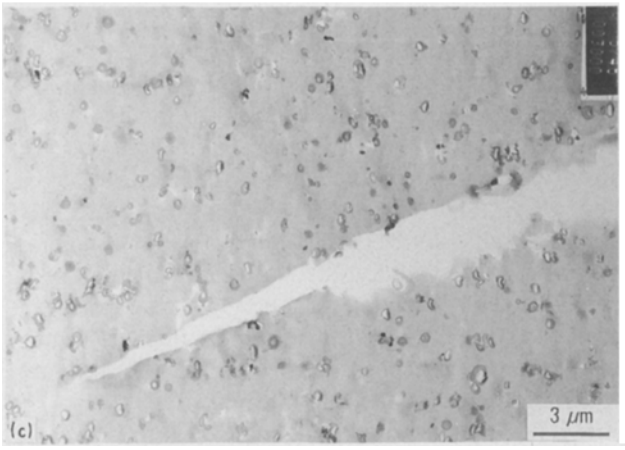

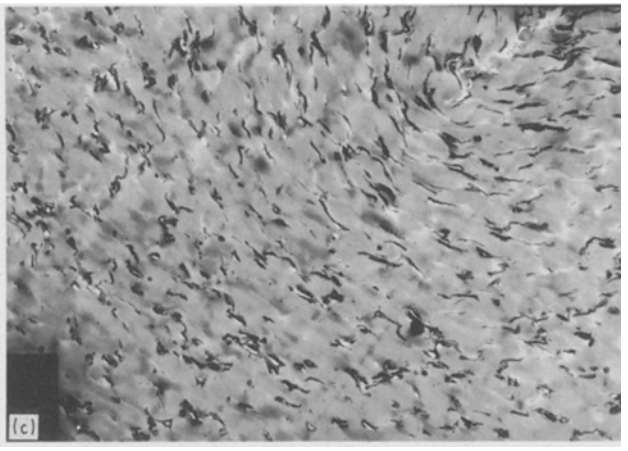

Figure 11 (a–c) Transmission electron micrographs taken from an ultra-thin section of an impact loaded specimen at room temperature. Fracture behaviour is seen to be only cavitation and crazing. No shear yielding is sighted. (a–c) correspond to locations indicated near the crack tip. Details are given in the text. (a) × 10 300.

Figure 12 (a–c) Transmission electron micrographs taken from an ultra-thin section of an impact-loaded specimen at 70 °C. Fracture behaviour is seen to be cavitation and shear yielding. No crazing is found. Crack tip is at the top right-hand corner of (c). Details are given in the text. (a) × 13 600, (b) × 10 300, (c) × 3000. 12(c).

rubbery inclusions together with severe crack-tip blunting.

Acknowledgements

The authors thank the Sydney University Electron Microscope Unit for placing its facilities at our disposal, and Bayer AG (Australia) for the supply of material for testing. The financial support from the Sydney University Postgraduate Research Award and a Junior Research Fellowship from the Australian Research Council to one of us (J. S. Wu) is greatly appreciated.

References

1. C. B. BUCKNALL, "Toughened Plastics" (Applied Science, London, 1977).
2. C. B. BUCKNALL and R. R. SMITH, *Polymer* **6** (1965) 437.
3. S. NEWMAN and S. STRELLA, *J. Appl. Polym. Sci.* **9** (1965) 2297.
4. S. STRELLA, *J. Polym. Sci. A2* **3** (1966) 527.
5. C. B. BUCKNALL, D. CLAYTON and W. E. KEAST, *J. Mater. Sci.* **7** (1972) 1443.
6. S. KUNZ-DOUGLASS, P. W. R. BEAUMONT and M. F. ASHBY, *ibid.* **15** (1980) 1109.
7. S. KUNZ and P. W. R. BEAUMONT, *ibid.* **16** (1981) 3141.
8. A. M. DONALD and E. J. KRAMER, *J. Appl. Polym. Sci.* **27** (1982) 3729.
9. S. WU, *Polymer* **26** (1985) 1855.
10. R. J. M. BORGGREVE, R. J. GAYMANS, J. SCHUIJER and J. F. INGEN-HOUSZ, *ibid.* **28** (1987) 1489.
11. S. WU, *J. Polym. Sci. Polym. Phys. Edn.* **21** (1983) 699.
12. A. F. YEE and R. A. PEARSON, *J. Mater. Sci.* **21** (1986) 2462.
13. R. A. PEARSON and A. F. YEE, *ibid.* **21** (1986) 2475.
14. D. S. PARKER, H.-J. SUE, J. HUANG and A. F. YEE, *Polymer* **30** (1989) 570.
15. T. FUKUI, Y. KIKUCHI and T. INOUE, *ibid.* **32** (1991) 2367.
16. A. F. YEE, W. V. OLSZEWSKI and S. MILLER, *Adv. Chem. Ser. Amer. Chem. Soc.* **154** (1976) 97.
17. A. F. YEE, *J. Mater. Sci.* **12** (1977) 757.
18. A. F. YEE and M. A. MAXWELL, *Polym. Engng Sci.* **21** (1981) 205.
19. W. D. BASCOM, R. Y. TING, R. J. MOULTON, C. K. RIEW and A. R. SIEBERT, *J. Mater. Sci.* **16** (1981) 2657.
20. F. SPERONI, E. CASTOLDI, P. FABBRI and T. CASIRAGHI, *ibid.* **24** (1989) 2165.
21. M. E. J. DEKKERS, S. Y. HOBBS and V. H. WATKINS, *ibid.* **23** (1988) 1225.
22. H.-J. SUE and A. F. YEE, *ibid.* **24** (1989) 1447.
23. A. G. EVANS, Z. B. AHMAD, D. G. GILBERT and P. W. R. BEAUMONT, *Acta Metall.* **34** (1) (1986) 79.
24. A. S. ARGON, in "Advances in Fracture Research ICF7", Proceedings of the 7th International Conference on Fracture, edited by K. Salama, K. Ravi-Chandar, D. M. R. Taplin and P. Rama Rao, Vol. 4 (Pergamon Press, London, 1989) p. 2661.
25. F. J. GUILD and R. J. YOUNG, *J. Mater. Sci.* **24** (1989) 298.
26. A. J. KINLOCH and D. L. HUNSTON, *J. Mater. Sci. Lett.* **5** (1986) 909.
27. D. J. HOURSTON, S. LANE and H. X. ZHANG, *Polymer* **32** (1991) 2215.
28. H.-J. SUE, PhD thesis, The University of Michigan (1988).
29. K.-K. KOO, T. INOUE and K. MIYASAKA, *Polym. Engng Sci.* **25** (1985) 741.
30. L. M. ROBESON, *ibid.* **24** (1984) 587.
31. S. Y. HOBBS, M. E. J. DEKKERS and V. H. WATKINS, *J. Mater. Sci.* **23** (1988) 1219.
32. M. E. J. DEKKERS, S. Y. HOBBS and V. H. WATKINS, *Polymer* **32** (1991) 2150.
33. J. S. WU, Y.-W. MAI and B. COTTERELL, *J. Mater. Sci.* **28** (1993) ?.
34. K. KATO, *Polym. Engng Sci.* **7** (1967) 38.
35. J. S. TRENT, J. I. SCHEINBEIM and P. R. COUCHMAN, *Macromolecules* **16** (1983) 589.
36. D. DELIMOY, C. BAILLY, J. DEVAUX and R. LEGRAS, *Polym. Engng Sci.* **28** (1988) 104.
37. K. FRIEDRICH, in "Crazing in Polymers", Advances in Polymer Science, Vol. 52/53, edited by H. H. Kausch (Springer-Verlag, Berlin, 1983).
38. H. SCHORDIN, in "Fractures", edited by B. L. Averback (Wiley, New York, 1959) p. 298.

Received 27 October
and accepted 19 November 1992